Flip-Chip Integration of InP to SiN Photonic Integrated Circuits

Michael Theurer [ORCID], Martin Moehrle, Ariane Sigmund, Karl-Otto Velthaus, Ruud M. Oldenbeuving, Lennart Wevers, Ferry M. Postma [ORCID], Richard Mateman, Frederik Schreuder, Dimitri Geskus, Kerstin Wörhoff, Ronald Dekker, Rene G. Heideman, and Martin Schell

(Highly-Scored Paper)

Abstract—We present our hybrid InP to SiN TriPleX integration interface with a novel alignment technique and its application to complex photonic integrated circuits. The integration interface comprises vertical alignment stops, which simplify the alignment process and allow for array integration with the same simplicity as for single dies. Horizontal alignment is carried out by utilizing optical backscatter reflectometry to get an active feedback signal without the need to operate the chip. Thus, typical contacting limitations of active flip-chip alignment are overcome. By using this method, we demonstrate the integration of InP DFB lasers with more than 60 mW of optical power coupled to a SiN waveguide with an averaged coupling loss of -2.1 dB. The hybrid integration process is demonstrated for single dies as well as full arrays. We evaluate the feasibility of the assembly process for complex photonic integrated circuits by integrating an InP gain chip to a SiN TriPleX external cavity. The process proves to be well suited and allows monitoring chip quality during assembly. A fully functional hybrid integrated tunable laser is fabricated, which is capable of full C-band tuning with optical output power of up to 60 mW.

Index Terms—Flip-chip devices, hybrid integrated circuits, reflectometry, semiconductor lasers, silicon photonics.

I. INTRODUCTION

TO DATE, silicon based photonic platforms, such as silicon on insulator (SOI) or SiN TriPleX, have become mature technologies and are widely commercially available [1]–[4]. The development of these platforms from pure research to the commercial level was made possible by their excellent optical properties and accelerated by the prospect of immense cost reduction from using available silicon facilities for optical chip production. A broad device portfolio is offered by both platforms. SOI, due to its high index contrast, has its strength in low footprint devices and offers passive components as well as active components such as high-speed photodetectors and modulators [1], [2]. SiN TriPleX on the other hand is a pure passive platform that excels when it comes to extremely low loss devices and low susceptibility to phase errors [3], [4]. Since silicon and SiN lack a direct bandgap, both platforms require the integration of direct bandgap material, in particular III-V, to realize efficient optical sources. This can be achieved by two fundamentally different ways. One is to integrate III-V epitaxial layers on a wafer level by either direct epitaxial growth or bonding of wafer pieces on a silicon photonics wafer that is then further processed in the silicon fab for final fabrication of the hybrid-integrated device [5]–[7]. This approach has the advantage of a simple optical alignment based on lithographic accuracy and it allows for a high throughput as it is done on a wafer level. The downside is that compromises have to be made by combining the two material systems during processing which in turn limits overall device performance. The alternative approach is to fully process the silicon photonics and III-V chips individually and then carry out a hybrid integration step. This way, no compromises regarding processing have to be made, and only known good dies can be used for hybrid assembly. The biggest downside is that optical alignment is challenging, so a sophisticated assembly process is required to realize reliable and efficient hybrid-integrated devices. One of the first assembly processes in this direction to be commercially successful on a larger scale was the use of micro optical benches [8], [9]. This approach has proven to yield reliable hybrid-integrated devices but it is a complex process that requires the assembly of multiple parts. A simpler approach is to mount the III-V and silicon photonics chips on individual carriers and then butt couple the chips facets by gluing the chip edges together with index matching glue [10], [11]. This method is straight forward and yields good performing devices but the position of the coupling interface is limited to the chip edges which makes it incompatible for integration on wafer scale. In addition, the process requires the optical alignment to be carried out for all 6 degrees of freedom (3 translation & 3 rotation). A more sophisticated approach is to use butt coupling with on chip flip-chip integration [12]–[14]. Here, the III-V chip is
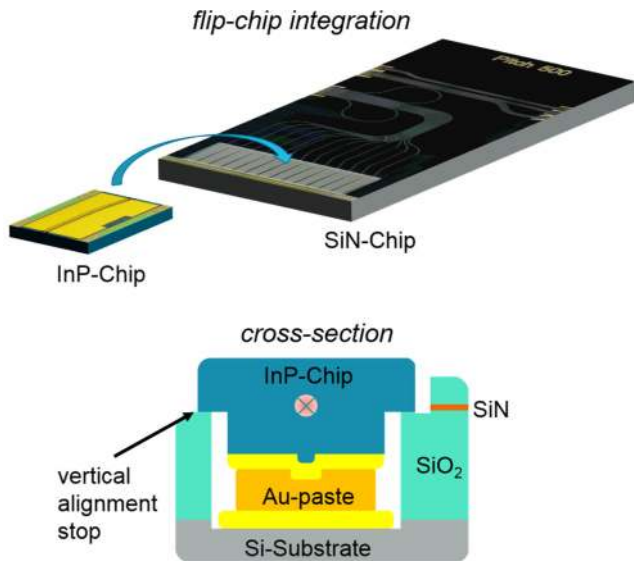
Fig. 1. Hybrid flip-chip integration of InP chip into etched recess on SiN TriPleX chip (top) and cross-section through InP chip bonded to SiN chip (bottom).

Fig. 2. Photograph of multiple single lasers (left) and a full laser 4-array (right) flip-chip integrated onto a SiN TriPleX chip [16].

flip-chip bonded into an etched recess on the silicon photonics chip. The facets are passively aligned in the vertical direction via mechanical alignment stops which simplifies the alignment process by cutting the number of degrees of freedom in half (2 translation & 1 rotation). The integration interface can be placed anywhere on the silicon photonics chip and is suitable for on wafer scale integration.

In our previous work, we presented our on chip flip-chip integration interface for coupling InP chips to SiN TriPleX and investigated different alignment processes [15], [16]. A novel alignment process utilizing optical backscatter reflectometry (OBR) proved as most successful. With what we call OBR alignment, we were able to demonstrate more than 60 mW of optical power coupled from a DFB laser to a single SiN waveguide structure. In this publication, we extend our previous findings by investigating OBR alignment for complex photonic integrated circuits (PIC), in this case the external cavity of a hybrid tunable laser. We will show that OBR alignment is well suited for hybrid integration of such devices, too, and in addition allows monitoring the quality of the PIC during assembly so that faulty devices can be ruled out prior to the assembly.

II. Hybrid Flip-Chip Integration Interface

Our hybrid integration interface is designed for on-chip flip-chip integration as shown at the top of Fig. 1. The InP chip is bonded in a p-side down configuration into an etched recess on the SiN TriPleX chip. To provide good heatsinking the recess is etched through the silicon oxide layer down to the silicon substrate as shown in the cross-section at the bottom of Fig. 1. An Au-paste composed of sub-micron size Au powder (AuRoFUSE[TM], Tanaka Kikinzoku Kogyo Co., Ltd.) was applied to the TriPleX Au-contact pads for bonding [17]. The TriPleX and InP chip have precise mechanical alignment stops
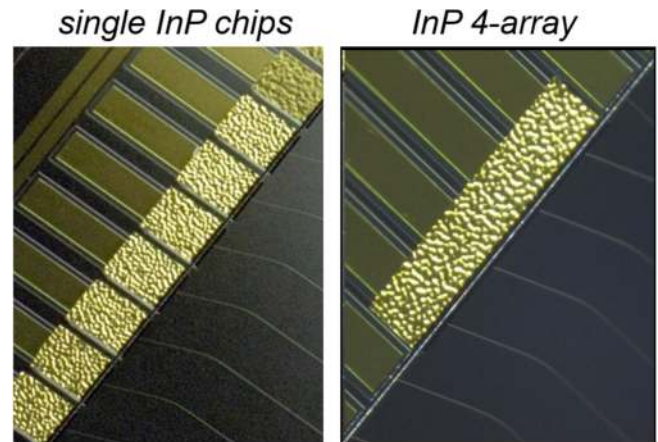
for passive alignment in the vertical direction and two rotational axes. At the interface facets, the chips have integrated spot size converters (SSC) for mode matching and increased alignment tolerances. The InP chips are 700 μm long and comprise a buried hetero structure. They were fabricated as DFB lasers for full InP laser integration and as gain chips for assembly of a hybrid tuneable laser. To prevent optical feedback from the interface facets, the waveguides of InP and SiN chips are tilted. The integration interface allows for the consecutive integration of several single InP chips as well as for full arrays (c.f. Fig. 2). Multiple InP chips can be integrated on a single TriPleX chip or wafer in an efficient way by consecutively optically aligning several InP chips followed by a single heating cycle to form the electrical and mechanical bond of all chips at once. To reduce the risk of misalignment, a short heating cycle to fixate the chips can be included after each optical alignment. Since the Au-paste bonding process requires no reflow, the Au-bond will stay solidified even for repeated heating cycles [17].

III. DFB Laser Integration

A. Alignment Process

A limiting factor for conventional active alignment techniques is the requirement to electrically contact the chips to get an active feedback signal. Using OBR alignment allows to overcome this limitation as the chip does not need to be operated to get the active feedback signal. An optical backscatter reflectometer (Luna OBR 4600) is connected to the output of the SiN TriPleX chip via a cleaved single mode fiber to give a measurement of the optical reflections as a function of the distance on the SiN chip. The measurement is based on wavelength-swept optical frequency domain reflectometry (OFDR). A wavelength range of 1601 nm to 1613 nm was chosen to minimize absorption in the C-band DFB laser chip. The alignment process is started by placing the DFB laser with a manual die-bonder (FINEPLACER lambda) on the integration interface with a rough pre-alignment based on the visual alignment marks. The chip then is passively vertically aligned by the mechanical alignment structures and
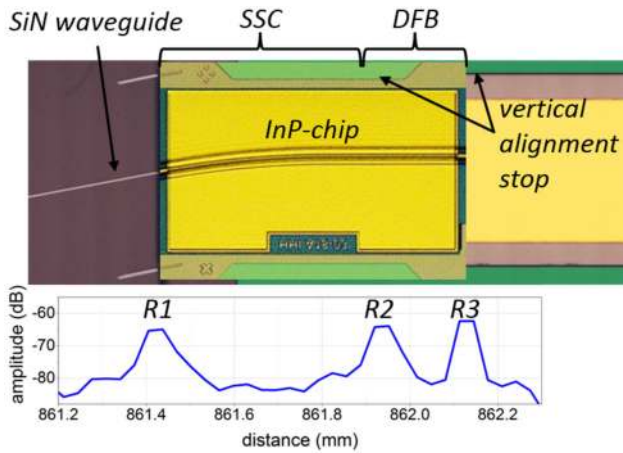
Fig. 3. Overlay image of fabricated InP chip and etched recess of SiN TriPleX chip, the vertical alignment stops are highlighted green (top). Reflection amplitude vs. distance (group index $n = 3.2$) measured with optical backscatter reflectometer (bottom) [16].
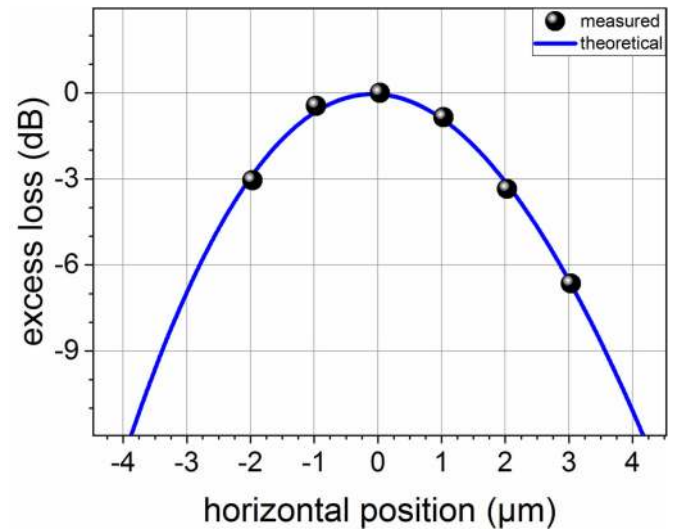

Fig. 4. Excess coupling loss for horizontal position. Measurements (circles) base on measured reflection amplitude R2 (c.f. Fig. 3 bottom). Theory (blue line) bases on Gaussian approximation [18] with MFD_{DFB} of 3.6 μm and 3 μm and $\text{MFD}_{\text{TriPleX}}$ of 4.2 μm and 4.4 μm in vertical and horizontal direction, respectively.

only horizontal alignment needs to be carried out. The bottom of Fig. 3 shows the measured OBR signal corresponding to the DFB laser shown in the overlay image at the top of Fig. 3. The signal shows three distinct reflections (R1-R3). R1 is related to the residual reflection of the TriPlex/InP interface. R2 indicates the beginning of the DFB grating. It should be noted that the used wavelength range is outside the DFB gratings stopband, so the reflection is not related to the stopband but to the effective index change from the grating. R3 stems from residual reflection of the in this case antireflection coated back facet. The amplitude of each reflection is proportional to the reflection coefficients as well as the optical losses on the path from and to the reflectometer. For R2 and R3 the optical losses include the chip to chip coupling loss and thus their amplitude R in dB can be expressed with the simple relation:

$$R = R' + 2\eta \qquad (1)$$

With η being the excess chip to chip coupling loss in dB due to horizontal misalignment and R' the reflection amplitude for optimum horizontal alignment. The excess coupling loss η has a factor of two as the light passes the interface facets twice on its way from and to the reflectometer.

Fig. 4 shows an example of the measured excess coupling loss based on the reflection amplitude of R2 at different horizontal positions of the DFB laser chip. The blue line shows the theoretical excess loss based on Gaussian approximation [18] with Gaussian mode field diameters (MFD) of 3.6 μm and 3 μm for the DFB laser and 4.2 μm and 4.4 μm for the TriPleX chip in vertical and horizontal direction, respectively. The MFD were derived from far field measurements as shown in [16]. The theoretical curve fits very well to the measurement and the optimum position can be clearly determined. The Au-paste was applied to the TriPleX bonding pad after which the chip was pressed onto the vertical alignment stops and the bonding tool was removed. The excess coupling loss was monitored during all of these steps and no change in loss was observed. The chip
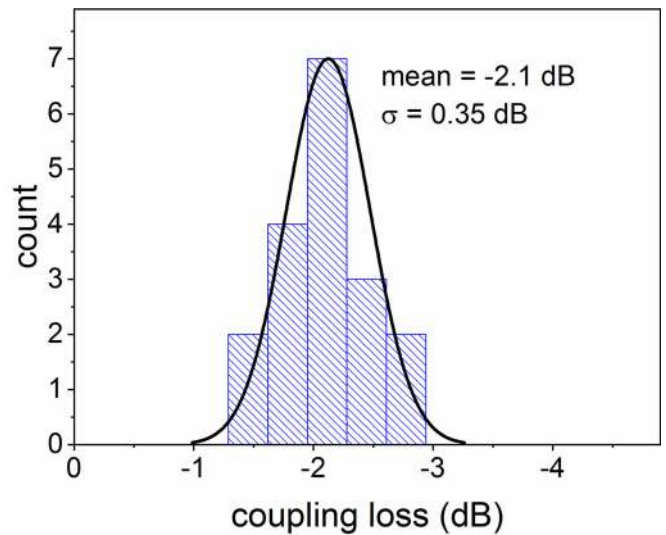

Fig. 5. Measured chip to chip coupling loss of 18 InP DFB lasers flip-chip integrated to SiN TriPleX using OBR alignment [16].

was then heated to 250 °C for sintering of the Au-paste to form a thermally and electrically highly conductive Au-Au joint. All alignment processes were carried out with a safety air gap of ∼6 μm between the TriPleX and InP facets to prevent facet damage.

The OBR alignment process was carried out for 18 InP DFB lasers. The chip to chip coupling loss was measured by comparing the pulsed output power at the laser facets before flip-chip assembly with the power coupled to the SiN waveguide after assembly (cf. Fig. 5). The average coupling loss was −2.1 dB with a standard deviation of 0.35 dB showing good reproducibility for the process. The theoretical coupling loss based on Gaussian approximation [18] is −1.3 dB, consisting
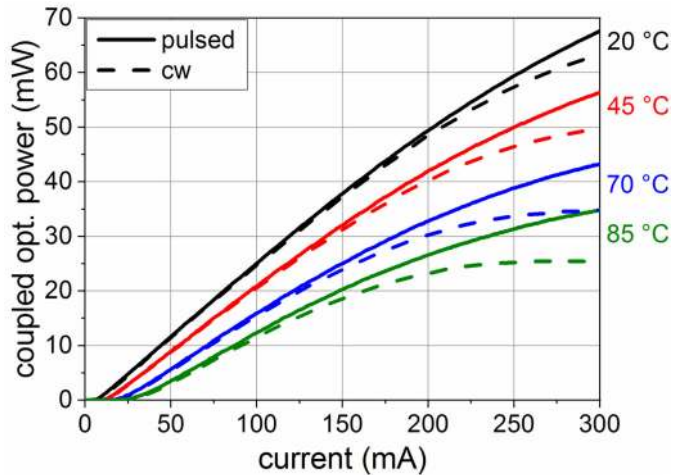
Fig. 6.   Optical power coupled to the SiN waveguide from a flip-chip integrated DFB laser for different heatsink temperatures in pulsed and cw operation [16].

Fig. 7.   Optical spectra of a flip-chip integrated DFB laser from 100 mA to 300 mA laser current at 20 °C and 85 °C heatsink temperature. The corresponding side mode suppression ratio is shown in the inset [16].

of −0.4 dB mode mismatch contribution and −0.9 dB from the 6 μm air gap. We believe that the difference of 0.8 dB between theory and experiment is due to non-perfect horizontal/vertical alignment, non-Gaussian beam shape, and residual reflections on the not AR-coated waveguide facets on TriPleX.

B. Single Integrated DFB Laser Performance

For single DFB lasers a high reflective coating was applied to the back facet to maximise output power at the front facet. The front facet was antireflection coated against air. No index matching filling material was used, as the tilted facets proved to sufficiently supress residual reflections for DFB lasers. The waveguide coupled optical power of a single DFB laser integrated with OBR alignment is shown in Fig. 6. A power above 60 mW is achieved at 20 °C heatsink temperature. Thanks to a direct thermal connection of the DFB laser to the silicon substrate the device can be operated up to 85 °C with waveguide coupled optical power up to 25 mW. For this device, a coupling loss of −1.6 dB was measured by comparing the pulsed output power of the laser facet before flip-chip assembly with the power coupled to the SiN waveguide after the assembly.

The measured optical spectra of the integrated DFB laser are shown in Fig. 7. As shown in the inset of Fig. 7, a stable side mode suppression ratio is maintained over the whole operation range. This shows that the optical reflection from the interface facets, which otherwise would lead to multimode behaviour, is sufficiently supressed by the waveguide tilt.

C. Integrated DFB Laser 4-Array Performance

For the DFB laser 4-array the back facet was antireflection coated to achieve the high single mode yield required for array structures. The hybrid integration process was carried out the same way as for single DFB lasers. A single device of the 4-array was aligned using the OBR alignment method and due to the passive vertical alignment, all other devices of the array are then automatically aligned as well. Fig. 8 shows the measured pulsed
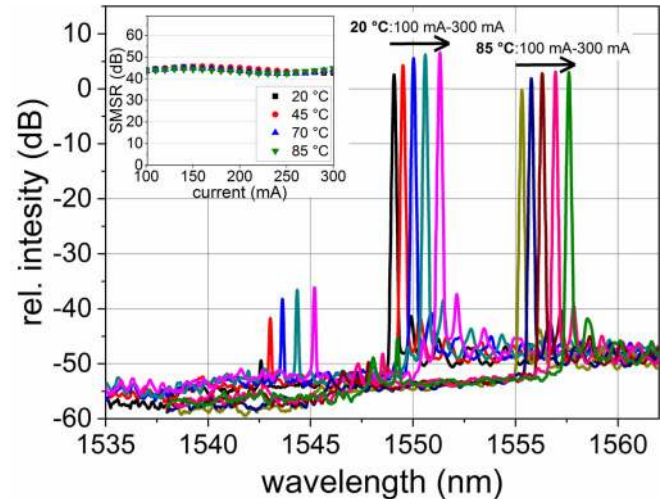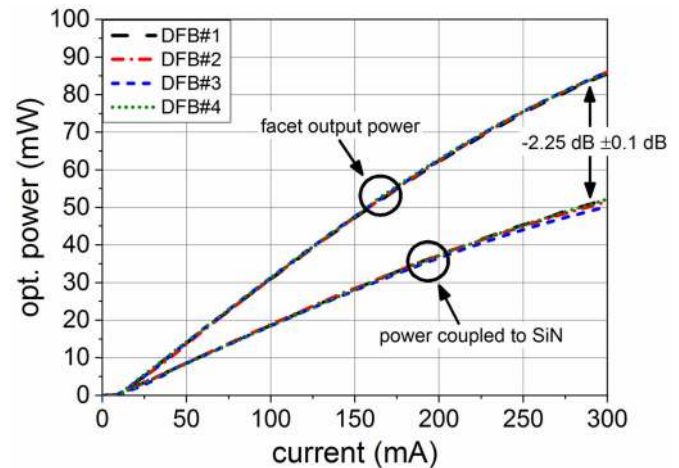

Fig. 8.   Pulsed output power of each laser in a hybrid integrated DFB laser 4-array at the laser facets before assembly and the power coupled to the SiN waveguides after assembly [16]. $T = 20$ °C.

output power of the lasers before flip-chip assembly and the power coupled to the SiN waveguide after the assembly. The array exhibits a high uniformity regarding output power and coupling loss. The averaged coupling loss of −2.25 dB varies by ±0.1 dB over the full array. This demonstrates well that thanks to the vertical alignment stops of the hybrid integration interface the alignment of a single laser is sufficient to align a full array and thus array integration can be performed with no added complexity compared to single dies.

IV. HYBRID TUNABLE LASER

A. Device Structure

Fig. 9 shows a schematic (top) and photograph (bottom) of the hybrid tunable laser comprising a TriPleX SiN Chip as external cavity and an InP gain chip flip-chip integrated to the hybrid
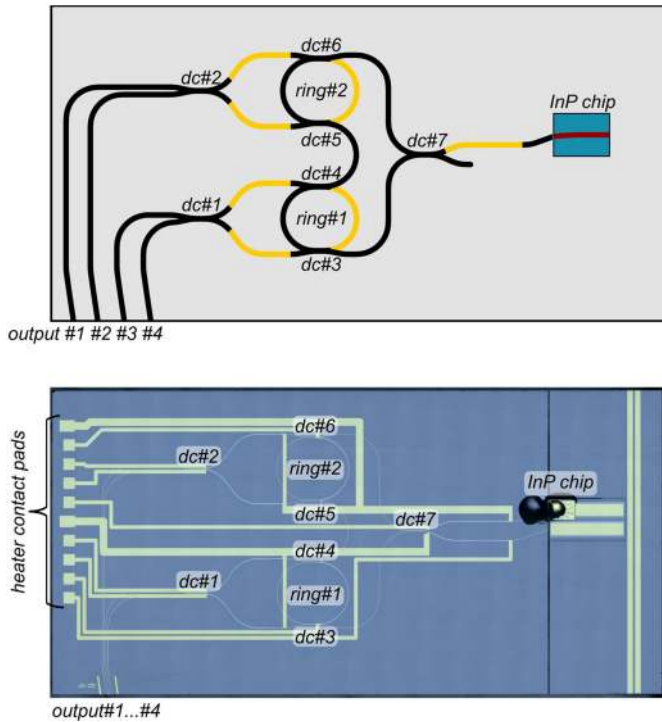
Fig. 9. Schematic (top) and photograph (bottom) of a hybrid integrated tunable laser chip with SiN TriPleX external cavity and InP gain chip. The SiN TriPleX chip consists of two ring resonators (*ring#1, #2*) and directional couplers (*dc#1-#7*) connected via optical waveguides. Heater electrodes (yellow in top) allow phase tuning of the ring resonators and the arms of the directional couplers (dc#1, #2, #7).
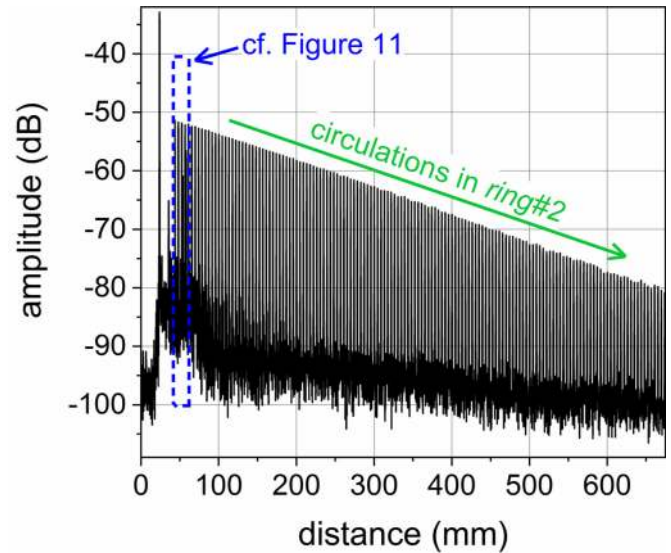

Fig. 10. Reflection amplitude vs. distance (group index $n = 1$) measured with optical backscatter reflectometer connected to *output#1* of hybrid tunable laser chip.

integration interface. To minimize undesired intra-cavity reflections, the front facet of the InP gain chip is antireflection coated against an refractive index of 1.5 which closely matches the refractive index of TriPleX. The air gap between the TriPleX and InP chips facets is filled with index matching UV-curable glue. The backfacet of the InP gain chip has a high reflective coating. The TriPleX chip comprises two ring resonators (ring#1, #2) in an add-drop configuration with two directional couplers (dc#4, #5) connected via a waveguide. Two ports of the outer directional couplers (dc#3, #6) are combined with an additional directional coupler (dc#7) with 3 dB power splitting ratio to form an optical cavity between the ring resonators and the InP chip. The ring resonators are designed with slightly different circumferences to exploit the Vernier effect to achieve a wide tuning range. The directional couplers (dc#3, #5, #6) have an identical design so that their coupling coefficient is the same and thus critical coupling occurs at resonance for ring#2 if waveguide losses are neglected. The directional coupler dc#4 on the other hand is designed to have a slightly higher coupling coefficient so that the critical coupling condition is not fulfilled and part of the light in the laser cavity is coupled out at ring#1. The outcoupled light is combined at dc#1 with a 3 dB power splitting ratio so by using the heaters for phase adjustment the output light can be combined to a single output waveguide (output#3 or #4). The two left output waveguides (output#1, #2) and dc#2 have no practical functionality apart from monitoring purposes. Both rings as well as two arms of each directional coupler have integrated heaters

to allow for phase tuning. Further information on similar hybrid tunable lasers can be found in [19], [20].

B. Optical Backscatter Reflectometry Signal

Fig. 10 shows the signal measured with the optical backscatter reflectometer connected to output#1 of the TriPleX chip. The high distinct peak at low distance stems from the fiber to chip interface. This peak is followed by a multitude of equidistant peaks that drop linearly in power. These equidistant peaks correspond to light which has coupled into ring#2 on one side (dc#5, #6) and coupled out on the other side (dc#6, #5) and then travels back to the reflectometer. Each consecutive peak stands for an additional circulation inside the ring, so that the distance between the peaks gives a direct measurement of the ring size for a known refractive index. By evaluating the distance for the given ring size we were able to derive a group index of 1.549 at 1550 nm. By measuring the drop in amplitude of the peaks, it is possible to derive the roundtrip loss of the ring. The measured roundtrip loss contains both the waveguide loss and the outcoupling loss of the two direction couplers and thus give a good measure on the quality of the ring structure. This allows to monitor the chips during the assembly process and to exclude faulty chips before bonding. Measuring the OBR signal with 1550 nm at output#1 / output#3 yields a roundtrip loss of -0.19 dB / -0.27 dB for ring#2 / ring#1, respectively. This corresponds well with the fact that dc#4 was designed to have a higher coupling coefficient than the other directional couplers.

Fig. 11 shows a close-up of the section marked blue in Fig. 10 with and without an InP chip placed on the integration interface and with and without index matching glue applied in the air gap between the facets. One can see three equidistant peaks that correspond to ring circulations as mentioned before and an additional peak around 54 mm marked R1. This peak corresponds to residual reflection from the TriPleX facet at the
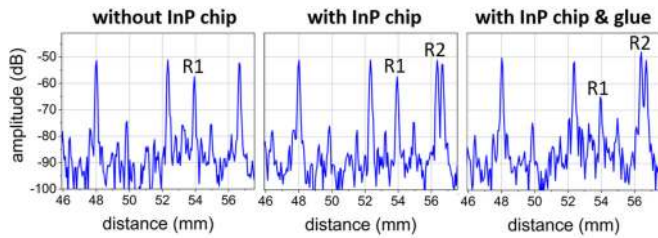
Fig. 11.　Close-up of section marked with blue dashed line in Fig. 10 with and without InP chip placed on integration interface or index matching glue applied. Reflection amplitude of TriPleX interface facet is marked as R1. Reflection amplitude of InP chip back facet is marked as R2. The three unmarked equidistant peaks correspond to circulations in *ring#2*.
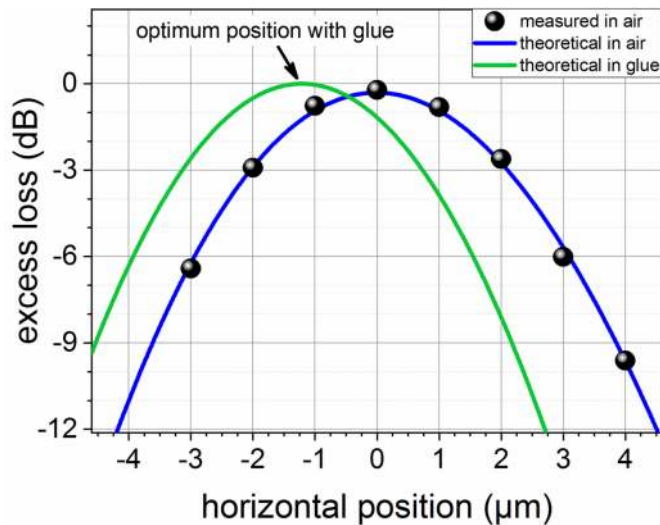

Fig. 12.　Excess coupling loss for horizontal position. Measurements in air (circles) base on measured reflection amplitude R2 (c.f. Fig. 11 middle). Theory in air (blue line) and in glue (green line) bases on Gaussian approximation [18] with MFD_{DFB} of 5.1 μm and 4.2 μm and $MFD_{TriPleX}$ of 4.2 μm and 4.4 μm in vertical and horizontal direction, respectively.

interface. When the InP gain chip is placed on the integration interface (cf. Fig. 11 middle) an additional peak R2 occurs which corresponds to the reflection of the InP chips back facet and can thus be used to get a relative measure of the coupling efficiency based on (1) to determine the optimum coupling position as described in Section III-A.

Fig. 12 shows the excess coupling loss based on the measured reflection amplitude R2 (c.f. Fig. 11) for different horizontal positions of the gain chip. The air gap between the facets was set to 6 μm as a safety distance. The theoretical loss (blue line) based on Gaussian approximation [18] fits very well to the measurement. Here Gaussian MFD of 5.1 μm and 4.2 μm were assumed for the InP gain chip in vertical and horizontal direction, respectively. The MFDs were extracted from far field measurements beforehand. When using index matching glue, it has to be taken into account that based on the law of refraction the output beam angle of the tilted facets will be different in air as to when index matching glue is applied. The green curve in Fig. 12 shows the theoretical excess loss for when index matching glue is used. The optimum position is shifted by about −1.25 μm and the theoretical coupling loss is reduced by about 0.3 dB.
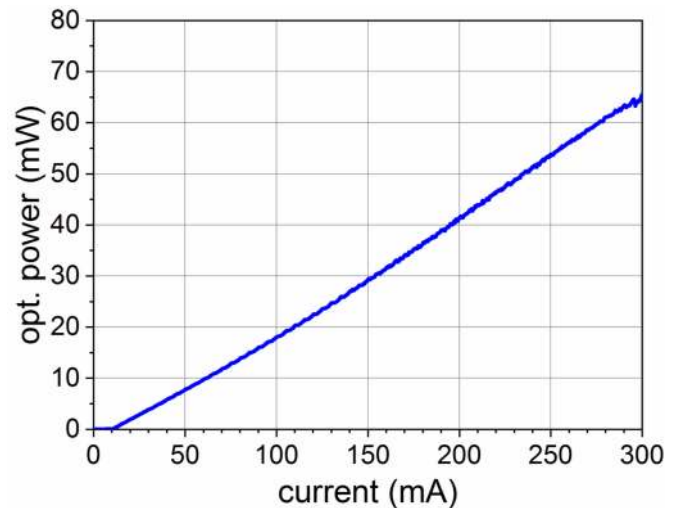

Fig. 13.　Pulsed output power vs. gain chip current of hybrid integrated tunable laser measured at output ports with integrating sphere. $T = 20$ °C.

The reduction in coupling loss comes from the reduced beam divergence in glue compared to air so that the 6 μm gap between the facets has less impact. Based on the theoretical curve, the chip was placed at the optimum position for glue and bonded to the TriPleX chip with Au-paste as described for the DFB lasers. The measured OBR signal directly after bonding is shown in Fig. 11 middle and the signal after applying the index matching glue is shown on the right. One can observe a drop of the reflection amplitude R1 from the TriPleX facet due to the index matching. The amplitude of R2 on the other hand is increased by about 3 dB which corresponds to 1.5 dB reduction of coupling loss. This is in good agreement with the theoretical curves shown in Fig. 12. For the gain chip of the hybrid tunable laser the theoretical chip to chip coupling loss with Gaussian approximation amounts to −0.3 dB which is 1 dB better than for the DFB laser. This is due to better mode matching and smaller beam divergence of the gain chips optical mode. There is no straight forward measurement of the real coupling loss for integrated gain chips but based on the results for measured and theoretical coupling losses of the DFB lasers we estimate that the real chip to chip coupling loss for the gain chips should be on average about −1 dB to −1.5 dB.

C. Hybrid Tunable Laser Performance

Fig. 13 shows the pulsed output power versus the current applied to the integrated gain chip in a free running configuration, i.e., without phase adjustment via the heaters. The power was measured at the output ports with an integrating sphere. The tunable laser exhibits a threshold current of 10 mA and an output power exceeding 60 mW at 300 mA.

To evaluate the basic tuning capability of the device the heaters of the rings were individually biased and the spectra measured at *output#4* (cf. Fig. 14). With heater currents up to 25 mA (19.5 V) a tuning range of 39 nm, covering the whole C-band, was achieved. A side mode suppression ratio above 50 dB is maintained over the full tuning range. The relative output power varies up to 1.5 dB. By tuning the heaters on the arms of *dc#1*
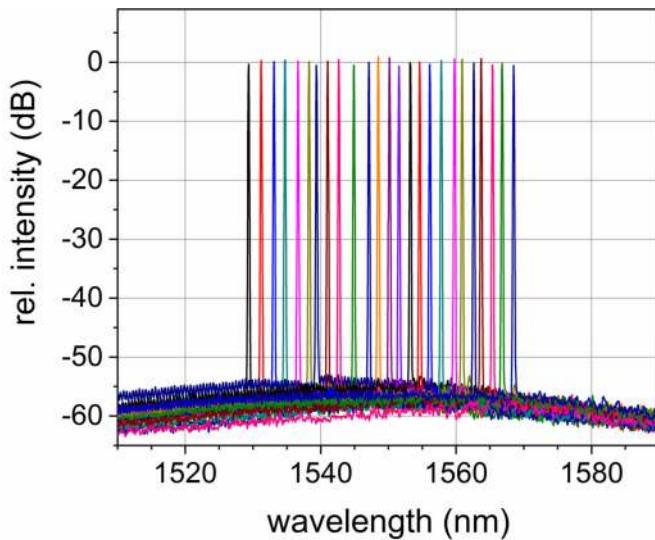
Fig. 14. Superposition of optical spectra at different tuning currents for hybrid integrated tunable laser measured at *output#4*. Maximum tuning current of *ring#1* and *ring#2* was 25 mA (19.5 V) each. Current applied to gain chip was 100 mA. $T = 20\ °C$.

the output power of the *output#3* and *#4* could be adjusted and the power equalized.

V. CONCLUSION

We demonstrated our hybrid III-V/SiN flip-chip integration interface together with a novel alignment technique based on optical backscatter reflectometry. We show the integration of DFB lasers to SiN waveguides with high reproducibility with an average coupling loss of -2.1 dB and SiN waveguide coupled optical power exceeding 60 mW. Due to its passive vertical alignment, the integration interface is also compatible for full array integration with no added complexity. The array shows high uniformity with a variation of coupling loss of less than 0.1 dB. We demonstrate the feasibility of the OBR alignment method for alignment of complex PICs by successfully integrating an InP gain chip to an SiN TriPleX external cavity chip. The hybrid tuneable laser exhibits a threshold current of 10 mA and an output power above 60 mW. With a tuning range of 39 nm it is capable of full C-band tuning. The OBR alignment method proves well suited for alignment of complex PICs and additionally allows monitoring the quality of the PIC to exclude faulty chips before hybrid assembly. We believe the hybrid flip-chip integration interface together with the OBR alignment method provides an efficient solution for hybrid chip integration

and could be readily adapted to other platforms such as SOI or polymer.

REFERENCES

[1] X. Chen, C. Li, and H. K. Tsang, "Device engineering for silicon photonics," *NPG Asia Mater.*, vol. 3, no. 1, pp. 34–40, Jan. 2011.

[2] G. T. Reed, *Silicon Photonics: The State of the Art*, Hoboken, NJ, USA: Wiley, 2008.

[3] C. G. H. Roeloffzen *et al.*, "Low-Loss Si_3N_4 TriPleX optical waveguides: Technology and applications overview," *IEEE J. Sel. Top. Quantum Electron.*, vol. 24, no. 4, Jul./Aug. 2018, Art no. 4400321.

[4] K. Wörhoff, R. G. Heideman, A. Leinse, and M. Hoekman, "TriPleX: A versatile dielectric photonic platform," *Adv. Opt. Technol.*, vol. 4, no. 2, pp. 189–207, Apr. 2015.

[5] D. Liang, G. Roelkens, R. Baets, and J. Bowers, "Hybrid integrated platforms for silicon photonics," *Materials*, vol. 3, no. 3, pp. 1782–1802, Mar. 2010.

[6] S. Keyvaninia, M. Muneeb, S. Stanković, P. J. V. Veldhoven, D. V. Thourhout, and G. Roelkens, "Ultra-thin DVS-BCB adhesive bonding of III-V wafers, dies and multiple dies to a patterned silicon-on-insulator substrate," *Opt. Mater. Express*, vol. 3, no. 1, pp. 35–46, Jan. 2013.

[7] T. Komljenovic *et al.*, "Heterogeneous silicon photonic integrated circuits," *J. Lightw. Technol.*, vol. 34, no. 1, pp. 20–35, Jan. 2016.

[8] P. D. Dobbelaere *et al.*, "Packaging of silicon photonics systems," in *Proc. OFC*, San Francisco, CA, USA, Mar. 2014, Paper W3I-2.

[9] L. Carroll *et al.*, "Photonic packaging: Transforming silicon photonic integrated circuits into photonic devices," *Appl. Sci.*, vol. 6, no. 12, Dec. 2016, Art. no. 426.

[10] G. de Valicourt *et al.*, "Hybrid III-V/Silicon integration: Enabling the next generation of advanced photonic transmitters," in *Proc. OFC*, San Diego, CA, USA, Mar. 2017, Paper W3E-3.

[11] B. B. Buckley *et al.*, "WDM source based on high-power, efficient 1280-nm DFB lasers for terabit interconnect technologies," *IEEE Photon. Technol. Lett.*, vol. 30, no. 22, pp. 1929–1932, Nov. 2018.

[12] N. Hatori *et al.*, "A hybrid integrated light source on a silicon platform using a trident spot-size converter," *J. Lightw. Technol.*, vol. 32, no. 7, pp. 1329–1336, Apr. 2014.

[13] F. E. Doany *et al.*, "A four-channel silicon photonic carrier with flip-chip integrated semiconductor optical amplifier (SOA) array providing >10-dB gain," in *Proc. ECTC*, Las Vegas, NV, USA, May 2016, pp. 1061–1068.

[14] A. Moscoso-Mártir *et al.*, "Hybrid silicon photonics flip-chip laser integration with vertical self-alignment," in *Proc. Conf. Lasers Electro-Opt. Pacific Rim*, Singapore, Singapore, Jul. 2017, Paper s2069.

[15] M. Theurer *et al.*, "Flip-chip integration of InP and SiN," *IEEE Photon. Technol. Lett.*, vol. 31, no. 3, pp. 273–276, Feb. 2019.

[16] M. Theurer *et al.*, "Actively aligned flip-chip integration of InP to SiN utilizing optical backscatter reflectometry," in *Proc. ECOC*, Dublin, Ireland, Sep. 2019, Paper W.2.B.

[17] T. Ogashiwa, "New process of bonding LED and power electronics chips," *ATZelektronik Worldwide*, vol. 12, no. 1, pp. 58–63, Feb. 2017.

[18] W. B. Joyce and B. C. DeLoach, "Alignment of gaussian beams," *Appl. Opt.*, vol. 23, no. 23, pp. 4187–4196, Dec. 1984.

[19] T. Chu, N. Fujioka, and M. Ishizaka, "Compact, lower-power-consumption wavelength tunable laser fabricated with silicon photonic-wire waveguide micro-ring resonators," *Opt. Express*, vol. 17, no. 16, pp. 14063–14068, Aug. 2009.

[20] Y. Lin *et al.*, "Characterization of hybrid InP-TriPleX photonic integrated tunable lasers based on silicon nitride (Si_3N_4/SiO_2) microring resonators for optical coherent system," *IEEE Photon. J.*, vol. 10, no. 3, Oct. 2018, Art no. 1400108.